齒狀迴中體抑素表現細胞之遠端軸突投射標的

Synaptic Transmission between Long-Range Somatostatin-positive Dentate Interneurons and Remote Target cells

研究生：顏廷耘 (Ting-Yun Yen)

指導教授：連正章 博士 (Cheng-Chang Lien, M.D., Ph.D.)

國立陽明大學

神經科學研究所

碩士論文

Institute of Neuroscience

National Yang-Ming University

Master Thesis

中華民國壹佰零參年柒月

July, 2014

致謝

這本論文謹獻給為了獲得這些實驗數據而犧牲的小鼠們,謝謝你們即使在不願意的情況下也做為稱職的實驗動物，讓我使用你們的身體。

能夠完成這些實驗，我必須感謝 Lien Lab 的各個成員。感謝連老師的指導與資源提供，翁儒韻、李政達、侯文賢、許燦庭、江柏瀚、簡大鈞、劉于超、陳建錞、許至緯在適當時機的提點，詹筑方、陳亭伃、曹茵絪、陳玠汝、高敏華、林昱伶、謝瑀的陪伴，學姊黃嘉怡的雞蛋和吳煜舜的細胞，以及其中幾個特別要感謝的 Optogenetics 好夥伴: 陳玠汝、許燦庭、侯文賢。

除此之外，我也要感謝幫我口試的口試委員: 很阿莎力答應擔任召集人的孫興祥老師、在口試結束後給染色建議的曹美玲老師、注意到論文許多待修改處的林惠菁老師、以及我的老師連正章老師。

最後，我想感謝我的家人，謝謝你們讓我沒有什麼包袱的過生活，也謝謝幾個老朋友(就不點名了)，謝謝你們在我有情緒的時候提供發洩的出口。

顏廷耘 謹致於

國立陽明大學神經科學研究所

中華民國壹佰零參年捌月

Contents

Chinese Abstract

海馬迴是一個與學習記憶密切相關的核區，依其結構可分為齒狀迴與 CA 兩個區域。由大腦皮質而來的訊息經穿緣通路進入素有「海馬迴的大門」之稱的齒狀迴，再由齒狀迴進一步將訊息傳遞到海馬迴的其他核區。齒狀迴在結構上是一個層疊結構成的核區，包括分子層、顆粒細胞層與 hilus 區。齒狀迴由許多種細胞組成，其中為數最多的細胞是興奮性的顆粒狀細胞，再者則是抑制性的中間細胞。在過去的觀念中，齒狀迴的中間細胞屬於區域性的細胞，具有軸突局限於當區的特性。然而在 1980 年代，有研究指出：齒狀迴中體抑素表現之細胞具有軸突遠距離投射至對側齒狀迴的特性，也就是在這種細胞本體的同側與對側齒狀均有該種細胞的軸突。即使當時的研究已了解其軸突可投射至對側齒狀迴，截至今日，該種軸突在對側海馬迴的分布狀況與投射之目標細胞種類仍尚未明確。本研究利用光遺傳學與電生理方法在對側齒狀迴辨認此種軸突可能投射到的目標細胞。我發現此種軸突將會投射到對側齒狀迴不同種類的細胞，有趣的是，相較對側齒狀迴的顆粒狀細胞而言，對側齒狀迴的中間細胞傾向接收較快並且較強的抑制信息。這些證據支持雙側齒狀迴間的抑制信息能夠調控顆粒狀細胞因此或許能影響物體辨識等海馬迴相關的功能。

English Abstract

The hippocampus is a key brain structure best known for its role in learning and memory. The hippocampus is commonly divided into two main areas, the dentate gyrus (DG) and cornu ammonis (CA). Cortical information is transferred to the DG, the primary gate of the hippocampus, through perforant paths (PPs) and further relayed to other hippocampal areas. The DG is a well-laminated structure composed of the molecular layer (ML), the granule cell layer (GCL), and hilus (HI). The DG contains heterogenous types of neurons including glutamatergic excitatory principal neurons, granule cells (GCs), and GABAergic inhibitory interneurons (INs). Traditionally, GABAergic INs in the DG are thought to be local-circuit neurons with their axonal arborization in the local areas. While in the 1980s, a class of somatostatin-expressing (SOM^+) neurons were found with characteristic of long-range projecting property. The axonal terminals of these neurons were found in both ipsilateral and contralateral of DG. Although the location of axonal projections has been found, their projection pattern and potential targets remain unknown. In this research, I combined optogenetics and electrophysiology to identify the targets of these long-range projection SOM^+ neurons in the contralateral hemisphere. Our results showed that synaptic efficacies and connectivity of SOM^+ neuron-mediated projections to the contralateral DG are target cell type-specific. Intriguingly, contralateral INs (cINs) receive stronger and faster inhibition but shorter synaptic latencies than GCs (cGCs). These evidence suggests that inter-DG inhibition contributes to modulation of GC input-output relations and may be involved in DG-dependent learning and memory such as pattern separation and completion.

Abbreviations

AAV, adeno-associated virus

ChR2, channelrhodopsin 2

CTB, cholera toxin B subunit

DG, dentate gyrus

GC, granule cell

HIPP cell, hilar perforant path-associated cell

HICAP cell, hilar commissural-associational pathway-associated cell

IN, interneuron

IPSC, inhibitory post-synaptic current

IML, inner molecular layer

MWW, Mann-Whitney-Wilcoxon

OML, outer molecular layer

PP, perforant path

R_{in}, input resistance

SOM, somatostatin

TML cell, total molecular layer cell

Introduction

The hippocampus

The hippocampus is a critical brain structure for learning and memory (Scoville and Milner, 1957; O'Keefe and Nadel, 1978). The hippocampus is named after its anatomical resemblance to the seahorse, from the Greek "hippos" for horse and "kampos" for sea monster). The hippocampus is a well-laminated structure which comprises two parts, the dentate gyrus (DG) and hippocampus proper (Cornu Amonnis [CA], commonly divided into CA1, CA2, and CA3 areas). The DG is the first relay station and serves as a primary gate of the hippocampus, which receives the inputs mainly from the entorhinal cortex layer II through the perforant paths, PPs. The principal cells in the DG, granule cells (GCs), send their axons, termed mossy fibers, toward the CA3 area. The highly specialized axonal outputs of mossy fibers provide strong synaptic excitation onto CA3 principal cells (Geiger and Jonas, 2000; Rollenhagen et al., 2007). The CA3 area is the next step in the progression of connections, and CA3 pyramidal cells give rise to their projections called Schaffer collaterals that innervate the apical dendrites of CA1 principal cells (Schaffer, 1892; Szirmai et al., 2012). The CA1 area is the output station of the hippocampus. Finally, CA1 principal cells project to the subiculum and other brain regions including the entorhinal cortex (Naber and Witter, 1998; Ishizuka, 2001). Thus the entorhinal-hippocampal circuit forms a loop processing unit and computes the cortical information.

DG microcircuits

As the gate of the hippocampus, information from the entorhinal cortex layer II enters the DG through the PPs. The PPs innervate GCs and local interneurons (INs). The axon collaterals of GCs innervate mossy cells and INs in the hilus. The mossy cells form commissural-associational projections to

innervate the GCs of the ipsi- and contralateral DG (Nakashiba et al., 2008).

GABAergic neurons in the DG

Depending on their axonal projections onto somatodendritic domains of principal cells, INs have been classified into perisomatic and dendritic inhibitory cells (Freund and Buzsáki, 1996). The functional properties of perisomatic inhibitory synapses of parvalbumin-expressing basket cells (BCs) are well described in the DG (Klaushaar and Jonas, 2000; Nörenberg, et al. 2010; Freund and Katona, 2007). Transmission at these synapses is characterized by a fast time course and large conductance (Bartos et al., 2002, 2007; Glickfeld and Scanziani, 2006) allowing precise control of timing and probability of spike generation in target cells (Pouille and Scanziani, 2001). These characteristics critically contribute to the synchronization of principal cells and the generation of fast network oscillations (Cobb et al., 1995; Buzsáki and Draguhn, 2004; Klausberger and Somogyi, 2008). Dendritic inhibitory neurons including somatostatin-expressing (SOM^+) hilar perforant path-associated cells (HIPPs), cholecystokinin-expressing hilar C/A path-associated cells (HICAPs), and total molecular layer interneurons (TMLs). Dendritic inhibition is proposed to control electrogenesis, synaptic plasticity, and activity states in their targets (Miles et al., 1996; Chiu et al., 2013; Xu et al., 2013; Hosp et al., 2014).

Commissurally projecting inhibitory INs in the DG

Conventionally, the word “interneuron” refers to the neuron with its local axonal innervation property. As early in 1980s, scientists used retrograde tracers and found glutamic acid decarboxylase-immunoreactive neurons in the hilus of rat hippocampal DG with commissurally projecting property (Ribak et al., 1986). They further found that some commissurally projecting neurons are also SOM-expressing neurons (Ribak et al., 1986; Zappone and Sloviter, 2001). Such neurons with both SOM^+

and long-range projecting properties were also been found in mice (Melzer et al., 2012), while the function of the long-range inhibition remains unknown.

Specific Aims

With anterograde and retrograde tracing methods, scientists provided several pieces of anatomical evidence for the existence of long-range projecting SOM^+ GABAergic neurons (Ribak et al, 1986). Because of the limited resolution of traditional immune-staining methods, the pattern of their axonal arborization and their postsynaptic targets remained unclear. The **Aim 1** of this study is to identify the postsynaptic neuronal targets, and to understand the SOM^+ neurons-mediated inhibition at a circuit and behavioral levels.

SOM^+ GABAergic neurons in the DG are mainly HIPPs (Freund and Buzsáki, 1996). The HIPPs form synapses with the distal dendrites of GCs. From our preliminary results, we concluded that 20% of SOM^+ neurons have the inter-DG projecting property. The **Aim 2** of this study is to identify the inter-DG inhibiting neurons and to compare them with other SOM^+ neurons.

Materials and Methods

Animals

We used both male and female *Sst*$^{tm2.1(cre)Zjh}$*/J* mice (013044, Jackson Laboratory) (hereafter called SOM-cre) over postnatal 30 days (P30) for neuronal tracing and optogenetic experiments. Animals were handled according to the national and institutional guidelines. All procedures were approved by the Animal Care and Use Committee of the National Yang-Ming University.

Virus preparation

We generated ChR2-expressing viruses in our lab or obtained them from the University of North Carolina Core (UNC) vector core (http://genetherapy.unc.edu/services.htm). The available viral vectors are shown in our lab website (http://lienlabnas.ym.edu.tw/lienlabwebsite/index.files/Page705.htm). All transgene constructs are gifts from Dr. Karl Deisseroth (Standford University, CA). The viral packaging and helper constructs are gifts from Dr. Lee, Jeng-Shin, Harvard Gene Therapy Initiative, Harvard Medical School, Boston, MA. Generation and purification of rAAVs were performed in our collaborator Dr. Tai, Min-Hong's laboratory in the National Sun Yat-Sen University.

Stereotaxic injection

Mice (postnatal day > 30) were anaesthetized with 4% isoflurane (vol/vol) in oxygen in the induction chamber (air flow rate: 4 ml/min), and then the head was shaved. Mice were placed onto the stereotaxic frame (Stoelting, Wood Dale, Illinois, USA). Animal's mouth and nose were immersed into the

anaesthetizing mask with constant 1.5% isoflurane air flow (air flow rate: 4 ml/min). A homeothermic blanket (Panlab Harvard apparatus, Cornella, Spain) was placed below the mice to keep the body temperature constant (36 ˚C). After securing the head with two ear bars, 75% ethanol was used to disinfect the surgical area and the animal's eyes were protected by ophthalmic gel. For targeting DG SOM-expressing neurons of the dorsal hippocampus, the midline scalp incision (~1 cm) was made by scissors and the skin was pulled aside to expose the skull. A small craniotomy was made corresponding to the location above the dorsal hippocampus (coordinates relative to the Bregma: AP: -2 mm; ML: 1.8 mm; DV: -2 mm and -1.8 mm). High titers of rAAV5-EF1a-DIO-hChR2(H134R)-eYFP-WPRE-hGH were delivered through the craniotomy using a 10μl NanoFil syringe (World Precision Instruments, Sarasota, Florida, USA) and a 35-gauge beveled metal needle. Injection volume (0.5 μl at each location) and the flow rate (0.1 μl/min) was controlled with a nanopump controller (KD Scientific, Holliston, Massachusetts, USA). After injection, the needle was left in place 0.1 mm above injection sites for 10 minutes before being withdrawn slowly. Following viral injections, we kept the mice in their home chamber ≥ 4 weeks to allow the maximum ChR2 expression.

For retrograde tracer injections (Red Retro Beads; Lumafluor; Cholera toxin B subunit-biocytin conjugates; Molecular probes), with an optimal injection volume 0.05μl at the same location as the virus injection. Following the retrograde tracer injections, we kept the mice in their home chamber for at least 3 to 5 days.

Electrophysiology and optical stimulation

Coronal brain slices of 300 μm thickness containing both DG were prepared from AAV-injected SOM-cre mice using a vibratome (DTK-1000, Dosaka, Kyoto, Japan). All animals were sacrificed by decapitation or by transcardial perfusion. The brains were rapidly removed and slices were cut in ice-

cold cutting saline containing (in mM): 87 NaCl, 25 $NaHCO_3$, 1.25 NaH_2PO_4, 2.5 KCl, 10 glucose, 75 sucrose, 0.5 $CaCl_2$ and 7$MgCl_2$. Brain slices were incubated in the oxygenated (95% O_2/ 5% CO_2) cutting saline in a recovery chamber at 34 ˚C for 30 min, and stored at room temperature until used, all procedure were performed under low light conditions. During experiments, slices were placed in a recording chamber and perfused with oxygenated artificial cerebral spinal fluid (ACSF) containing (in mM): 125 NaCl, 25 $NaHCO_3$, 1.25 NaH_2PO_4, 2.5 KCl, 25 glucose, 2 $CaCl_2$ and 1 $MgCl_2$. Expression of ChR2-eYFP was confirmed by epifluorescence and the neurons were visually selected for recordings under infrared differential interference contrast (IR-DIC) microscope (BX51WI; Olympus). ChR2 was excited by optical stimuli at 470 nm, which was delivered directly from the objective, the optical stimuli were simultaneously recorded by a GaP photodiode (wave length range: 150-550 nm, 1ns rise time, Thorlabs).

Whole-cell recordings were made using a Multiclamp 700B amplifier (Molecular Devices, Sunnyvale, CA, USA). Recording electrodes (2-5 MΩ) were pulled from borosilicate glass with filament (outer diameter, 1.5 mm; wall thickness, 0.32 mm; Harvard Apparatus, Edenbridge, UK). For performing patch-clamp recordings on potential post-synaptic neurons, recording pipets were filled with high Cl^- internal solution containing the following (in mM): 15 K-gluconate, 140 KCl, 0.1 EGTA, 2 $MgCl_2$, 4 Na_2ATP, 10 HEPES, and 0.4% biocytin (wt/vol) (osmolarity: 310 mOsm/L). For recordings on ChR2-eYFP-expressing neurons, recording pipets were filled with internal solution containing the following (in mM): 120 K-gluconate, 24 KCl, 0.2 EGTA, 4 MgATP, 10 HEPES, 7 Na_2-phosphocreatine, 0.5 NaGTP, and 0.4% biocytin (wt/vol). For all recordings, pipette capacitance was almost fully compensated. Series resistance (R_s) was compensated to ~80% in the voltage-clamp configuration. Signals were low-pass filtered at 4 kHz and sampled at 10 kHz using Digidata 1440A (Molecular Devices). A Digidata 1440 A connected to a personal computer was used for stimulus generation and data acquisition. Pulse sequences were generated by pClamp 10.2 (Molecular Devices). All recordings

were made at 22-24˚C.

Biocytin filling and reconstruction

For morphological analysis of electrophysiologically identified target cells, we filled whole-cell patch-clamped neurons for up to 30 min with biocytin (4 mg/ml, dissolved in intracellular solution). Subsequently, sections were fixed overnight in 4% paraformaldehyde, washed and stored in 0.1 M PBS. After washing with 0.1 M PBS, slices were incubated with Alexa 594 or Alexa 350 conjugated avidin (1:400; Invitrogen, Carlsbad, CA, USA) in 0.1 M PBS and 0.3% triton X-100 overnight at 4˚C. After wash, slices were embedded in mounting medium Vectashield (Vector Laboratories, Burlingame, CA, USA). Labelled neurons were examined by a two-photon microscope using a pulsed titanium: sapphire laser (Chameleon-Ultra II tuned to 800 nm for Alexa-594 and 720 nm for Alexa 350; Coherent, Portland, OR, USA) attached to a Leica DM6000 CFS (Leica, Wetzlar, Germany) that was equipped with a 20x/1.0 numerical aperture (NA) water immersion objective (HCX APO L; Leica, Wetzlar, Germany).

Immunohistochemistry

For identification of long-range projecting SOM^+ neurons, we used SOM-cre mice with unilatateral-hemispheric injection with AAV5-DIO-ChR2-eYFP into dorsal DG and injected CTB-biotin in the other hemispheric dorsal DG at least 3 days before performing the experiment. The animals were kept in their home chamber for at least 3 days after the injection of CTB-biotin. Trans-cardiac perfusion with 4% PFA were performed, the brain was then removed and soaked in 4% PFA for another 4 hours for further fixation. The brain was transferred into 15% sucrose in 0.1 M PBS overnight for dehydration and be kept in 30% sucrose in 0.1 M PBS for preservation. Frozen section of 40 μm thickness with cryostat microtome (Leica SM 2010R). Slices were permeabilized with 0.3% Triton-X 100 and then

blocked in 0.1 M PBS + 10% normal goat serum (NGS, 2 h at 4˚C). CTB-biotin conjugates were stained with Alexa 594 avidin conjugates (1:400; Invitrogen, Carlsbad, CA, USA). The primary antibody was applied in PBS + 0.3% Triton X-100 + 5% NGS (24 h at 4˚C), and the secondary antibody was incubated together with streptavidin conjugate in 0.1 M PBS + 0.3% Triton-X 100 + 2% NGS (2 h at 4˚C). After wash, slices were coverslipped with mounting medium Vectashield (Vector Laboratories, Burlingame, CA, USA). Slices were imaged by confocal microscopy (Leica DM6000 CFS).

Definition of the responsive postsynaptic cells

The criteria for defining a responsive cell is based on the averaged IPSCs (from at least 6 IPSCs). The cell was counted as a responsive cell only when its averaged IPSC amplitude is greater than 3-fold standard deviation (SD) of the baseline.

Data analysis

Data were analyzed using Clampfit 10.2 (Molecular Devices) and Prism 5.0 (GraphPad Software, San Diego, CA, USA).

Data were presented as mean ± standard error of mean (SEM). Error bars represent SEM. Statistical significance was tested by the Mann-Whitney-Wilcoxon (MWW) test at the significance level (P) as indicated using Prism 5.0.

Results

Long-range projecting SOM$^+$ neurons in the dorsal DG

To investigate the role of long-range projecting SOM$^+$ neurons in the dorsal DG, I initiated the experiments by providing anatomical evidence of long-range projecting SOM$^+$ neurons. Type 5 AAVs carrying double-floxed ChR2 fused with eYFP under the control of EF1a promoter were used to infect the unilateral side of dorsal hippocampal DG (Fig. 1A, 1B) of SOM-cre mice. The eYFP$^+$ somata could be observed mainly in the DG hilus (Fig. 1C, somata were indicated with stars), CA1 Stratum oriens (str. o), str. radiatum (str. r), str. lacunosum-moleculare (str. lm), and CA3 area in the virus injection side (Fig. 2B). Aside from the location of eYFP$^+$ somata, eYFP$^+$ neurites could be observed in the DG hilus, ML (Fig. 1C; 2B), CA1 str. o, str. r, and CA3 areas (Fig. 2B) in the ipsilateral side of virus injection. On the other hand, in the contralateral side of virus injection, eYFP$^+$ axons could be observed mainly in the DG hilus and ML. Sparse distribution of eYFP$^+$ axons was also observed in the CA1-3 areas (Fig. 2B).

To examine the somatic location of those SOM$^+$ neurons which mostly innervate the DG, I injected retrograde tracer, biotin-conjugated cholera toxin B subunit (CTB-biotin) into the AAV-ChR2 injected mice at least 25 days after virus injection (Fig. 2C). The CTB-biotin was injected specifically into the DG ML to avoid contamination to the CA1-3 areas (Fig. 3A, 3B). Signal of CTB-biotin was only observed in the DG hilus of the CTB-non-injected hippocampus (Fig. 3C$_1$) but not in the CA1-3 areas (Fig. 3C$_{2\text{-}4}$), suggesting that those neurons with axonal projections to contralateral DG were mainly located in the DG hilus. We found several CTB$^+$ neurons in the DG hilus of AAV-injected site (Fig. 3D$_{1\text{-}2}$), but only a small portion of them were also eYFP$^+$ (Fig. 3E$_2$). Approximately, 20% SOM$^+$

neurons in the dorsal DG hilus have the cDG projecting property (Fig. 3F).

Optical control of SOM^+ neurons

To study the target cells of long-range projecting SOM^+ axons, I used optogenetics and electrophysiology to study the functional connections between the long-range axons and their postsynaptic neurons (Fig. 4A, 4D). As illustrated (Fig. 4B, left), 1-ms pulses of blue light at 470 nm could reliably induce action potential in ChR2-expressing neurons. Action potentials were induced at 1.6 ms after the light pulse (Fig. 4B, right). One of the recorded $eYFP^+$ neuron was filled with biocytin and underwent reconstruction, its soma located in the border of GCL and hilus, and with its axons mostly in the OML, which is the typical morphology of HIPP.

I next determined whether the long-range axons make functional synapses onto neurons in the cDG by examining the photostimulation-induced postsynaptic responses in the cDG (Fig. 4D). The post-synaptic currents could be eliminated by bath application of gabazine (1μM) (Fig. 2E). One of the recorded cDG neuron was filled with biocytin and reconstructed (Fig. 4F). The light-induced $IPSC_1$ were plotted against different light intensity (from 0 to 100 %). The $IPSC_1$ recorded in several neurons (n = 4) showed that 10 % light intensity (that is, LED power equals to 2 mW) was sufficient to induce maximum postsynaptic responses (Fig 2G). To ensure reliable activation of the long-range axons, I used the maximum light intensity in the following experiments.

Identity of target neurons in the cDG

I recorded cGCs (51 cells) and cINs (32 cells). The cINs were classified into TML-like (3 cells), HIPP-like (3 cells), and HICAP-like (1 cell) cells based on the pattern of their axonal arborization, firing pattern, and input resistance (R_{in}) (Fig. 5). The TML cells have their axonal arborization in the ML,

with the average R_{in} of 247 MΩ (247 ± 30 MΩ; n = 3), and accommodating firing pattern. The HIPP cells have their axonal arborization mainly in the OML with an averaged R_{in} of 377 MΩ (377 ± 90 MΩ; n = 3). The HICAP cells have their axonal arborization mainly in the IML with the R_{in} of 260 MΩ (only one cell) (Hosp, et al., 2014). Many of the recorded cINs were failed to be reconstruct, in that case, I counted them as cINs (Fig. 6).

Several possible targets of long-range projecting SOM^+ neurons were identified, including DG GCs (13 cells of 51 cells were responsive to photo-stimuli), TML-like cells (2 cells of 3 cells), HIPP-like cells (3 cells of 6 cells), mossy cells, and CA3 pyramidal cells (Fig 3; data not shown).

Long-range projecting SOM^+ axons target both cGCs (-cGCs) and cINs (-cINs) with different synaptic strength and connectivity. The average IPSC measured on cINs was 38.6 ± 10.78 pA (n = 31), which was significantly greater than those measured on cGCs (11.4 ± 3.48 pA, n = 53; $p<0.001$; MWW test). The synaptic connectivity was also higher in -cINs than -cGCs (50% and 25.49%, respectively) (Fig. 6A-C). The synaptic latency and IPSC kinetics were differed between -cINs and -cGCs. The -cINs pathway had a shorter synaptic latency (2.6 ± 0.3 ms, n = 12) than -cGCs (3.4 ± 0.3 ms, n = 11). IPSC rise and decay time constant were faster in -cINs (0.64 ± 0.08 ms, and 9.4 ± 1.3 ms, respectively, n = 9) than in -cGCs (1.13 ± 0.2 ms, and 15 ± 2 ms, n = 7) ($p<0.05$) (MWW test) (Fig. 4D-G).

Discussion and Future work

Summary

From both anterograde and retrograde labeling, we have found a class of GABAergic projecting neurons in the DG, namely, long-range projecting SOM^+ neurons. These neurons are located in the dorsal DG hilus with their axonal arborization in the cDG ML and hilus. Combining electrophysiology with optogenetics, I discovered that these axons form inhibitory synapses with cGCs and several types of cINs, including TML and HIPP-like cells. The synaptic strength and connectivity of the long-range axons to cINs were both significantly higher than those to cGCs. Notably, synaptic latencies were significantly shorter in cINs than cGCs. Also, cINs had a faster IPSC kinetics than cGCs in both rise and decay time. In summary, the core findings of this study are: first, I found a class of SOM^+ neurons with long-range projecting property. Second, the targets of this long-range inhibition may include GCs and INs. Third, the synaptic strength of the long-range inhibition to cINs is larger than that to cGCs.

Identity of the long-range projecting SOM^+ neurons

To identify the long-range SOM^+ neurons, I injected Retro Beads (Red Beads IX) into the unilateral DG of GAD67-GFP mice. The GAD67-GFP mice express GFP in their GAD67-expressing neurons, including SOM^+ INs. With this experimental design, I could visualize the $GAD67^+$ neurons with GFP and performed whole-cell patch-clamp recordings of the GFP^+ and $Bead^+$ neurons (the long-range projecting neurons) in the Bead-non-injected site (Fig. 7). In this series of experiments, I have not found a neuron with both GFP and Beads. I have found some neurons with Beads and performed recordings of them (Fig. 7). The defect of this method is that the Beads will be diluted if I performed whole-cell recordings of the $Beads^+$ cells. To avoid this defect, I plan to unilaterally inject another

retrograde tracer, CTB-alexa 594. CTB is a membrane-anchored protein, the benefit of using it in the experiment is that it will not be diluted after whole-cell recordings, so I can reconstruct the morphologies of the long-range GAD^+ neurons. The drawback of using it is that the CTB might change the intrinsic properties of the neurons. I plan to acquire the morphologies of long-range projecting neurons by unilaterally injection of CTB-alexa 594 and to acquire the intrinsic properties of the neurons by Retro Beads injection. In the future, I plan to identify the long-range neurons with the offspring of SOM-cre crossed with Ai-14 mice to specifically study the identity of SOM^+ long-range neurons.

Possible function of long-range inhibition in dorsal DG

GABAergic INs in the DG are thought to control spatial learning and memory retrieval but not to affect memory retention (Andrews-Zwilling et al., 2012). SOM^+ neurons are a small population of GABAergic INs in the DG and they form inhibitory synapses with the distal dendrites of GCs, which resembles the O-LM neurons of the CA1 area. Dendritic inhibition in the CA1 had been proven to support fear learning through receiving cholinergic input from the medial septum (Lovett-Barron et al., 2014). We also want to know if the long-range projecting SOM^+ neurons will receive inputs from different origins or have other synaptic mechanisms than traditional HIPP neurons in the DG. To achieve this goal, we will inject Retro Beads into the other hemispheric DG of SOM-cre::Ai-14 mice and perform patch-clamp recordings to dig more into the different types of SOM^+ neurons in the DG.

To understand the function of SOM^+ neurons in the ipsilateral DG in the behavioral aspect, I plan to perform *in vivo* optogenetics to bilaterally silence SOM^+ axonal terminals (by bilaterally inject SOM-cre mice with AAV carrying halorhodopsin, AAV-NpHR) and examine several behavioral tests related to learning and memory. The first behavioral test I plan to perform the novel object recognition

test.

Role of long-range projecting SOM$^+$ neurons in DG microcircuits

Based on the synaptic latencies in the cDG, I summarized that the long-range axons form monosynaptic inhibitory synapses with cGCs and cINs. Also, comparing the long-range IPSC kinetics with the IPSC kinetics of dendritic inhibition in paired-recording studies in the DG local circuits (Liu et al., 2014; Savanthrapadian et al., 2014), I speculate that the long-range axons exhibits dendritic inhibition to the cells in the cDG.

Although the synaptic latencies of cINs is significantly shorter than that of cGCs, the difference is less than 1 ms, which is smaller than a monosynaptic transmission. These suggest the cGCs might first receive a feed-forward inhibition (SOM$^+$-cGCs)and after a brief time window, they will receive a feed-forward disinhibition (SOM$^+$-cINs-cGCs).

Dendritic inhibitory INs like the HIPPs are less likely to be recruit when an excitatory input enters the DG through the PPs (unpublished data, Lien Lab). If an excitatory input from the PPs is strong enough to excite HIPP, then several other types of neurons in the DG should also been recruited, including GCs. Based on the monosynaptic transmission between the long-range axon and cGCs and the spike probability of HIPPs, I hypothesize that the long-range SOM$^+$ neurons form feed-forward inhibition and feed-forward disinhibition to the cDG when a strong input enters the DG, generating a millisecond timescale inter-DG inhibition. This mechanism may contribute to the coordination of the two hemisphere.

Several experiments need to be done to further investigate the signal processing in the circuitry. First, it is necessary to control the ECII inputs to the DG. We plan to inject C1V1 opsin into the ECII,

the C1V1 opsin could be excited through 590 nm photo-stimuli; and unilaterally inject the ChR2 into the dorsal DG. With this design, we can record the GCs and INs in the non-injected dorsal DG, and use 470 nm and 590 nm photo-stimuli to study the associated signals from cDG and ECII.

SOM^+ neurons in the CA areas

In a subset of experiments, I injected the AAV-ChR2 into the CA1 or CA3 area. Intriguingly, the SOM^+ neurons in the CA1 area of the injection site also send their axons to the contralateral CA1 area. Notably, the pattern of axonal arborization is mostly in the str. r and str. o. Similar neuronal projections were also observed in the CA3 area. Collectively, I speculate that the SOM^+ neurons in a typical area (CA1, CA3, or DG) in the hippocampus send their axons to the counterpart area of the contralateral side.

The manipulation of SOM^+ neurons in the CA1 area is frequently linked to the epilepsy phenotypes. SOM^+ neurons in the CA1 area are reorganized in a model of epilepsy (pilocarpine-induced epilepsy) (Peng et al., 2013); they send their axons to the ML of DG and form inhibitory synapses with the GCs. To connect my findings to epilepsy, several experiments could be performed. First, we could use the pilocarpine-induced animal model in unilaterally CA1-injected (AAV-ChR2) SOM-cre mice and study the axonal density in the contralateral CA or DG. Second, we could optically manipulate the long-range axons in the CA1 area of the pilocarpine-treated and unilaterally CA1-injected (AAV-NpHR or AAV-ChR2) SOM-cre mice to monitor their epileptic behavior.

Figures

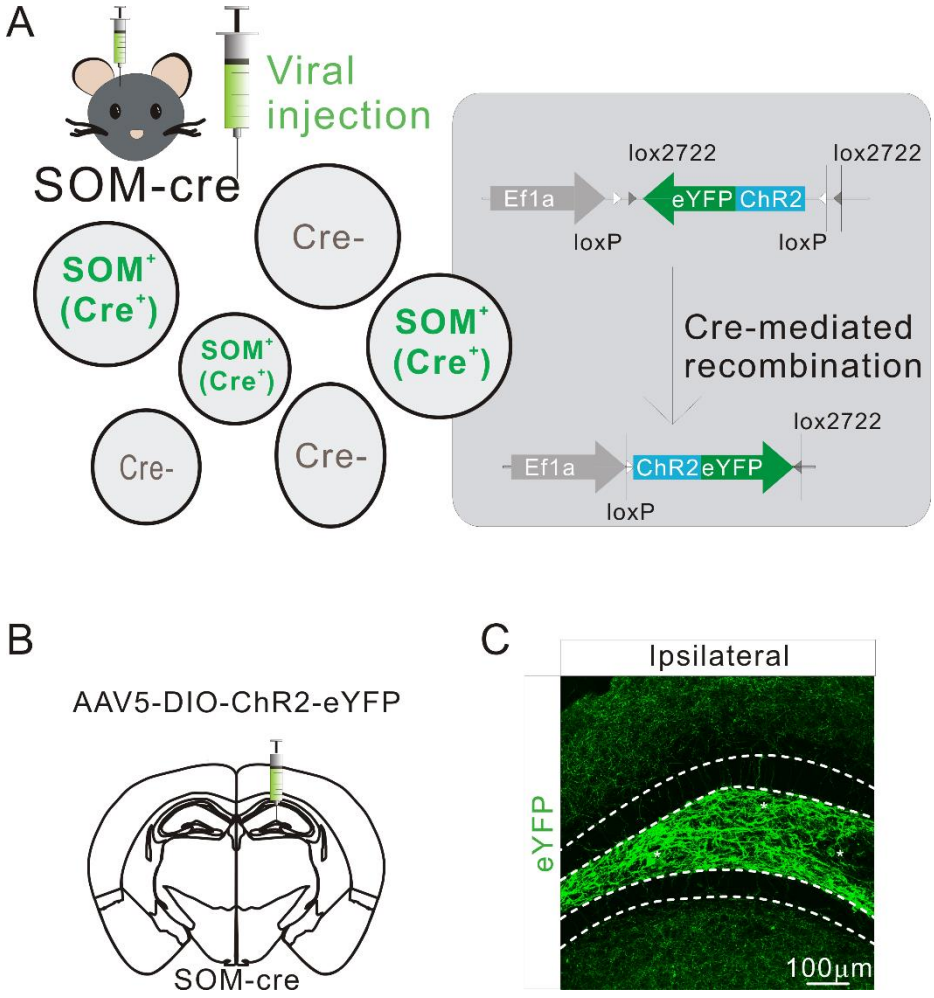

Figure 1. Expression of eYFP-tagged ChR2 in the DG

A, schema of injection of AAV5 carrying double-floxed inverted orientation (DIO) encoding ChR2-eYFP into the SOM-cre mice. The SOM^+ neurons of the injection site will express ChR2-eYFP through Cre-Lox recombination. B, schema of AAV5-DIO-ChR2-eYFP injection. The AAVs were injected into the right dorsal DG of SOM-cre mice. C, expression of eYFP-tagged ChR2 in the ipsilateral side of AAV injection. The borders of the DG GC layer were outlined. Somata of $eYFP^+$ neurons were indicated with stars.

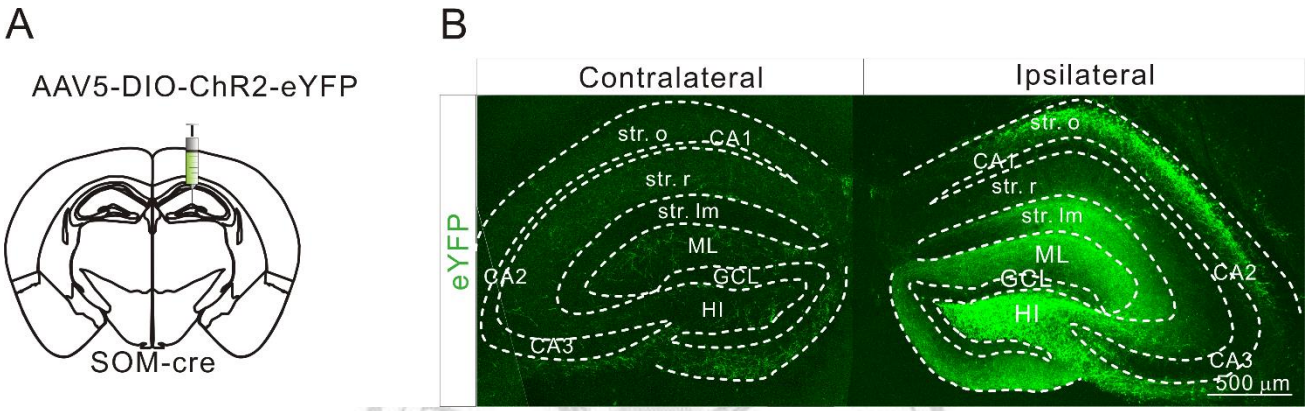

Figure 2. Long-range projecting SOM$^+$ neurons in the DG hilus

A, schema of AAV5-DIO-ChR2-eYFP injection. The AAVs were injected into the right dorsal DG of SOM-cre mice. B, expression of eYFP-tagged ChR2 in the ipsi- and contralateral side of AAV injection. The borders of laminated structure of the DG were outlined. (ML, molecular layer; GCL, granule cell layer; HI: hilus).

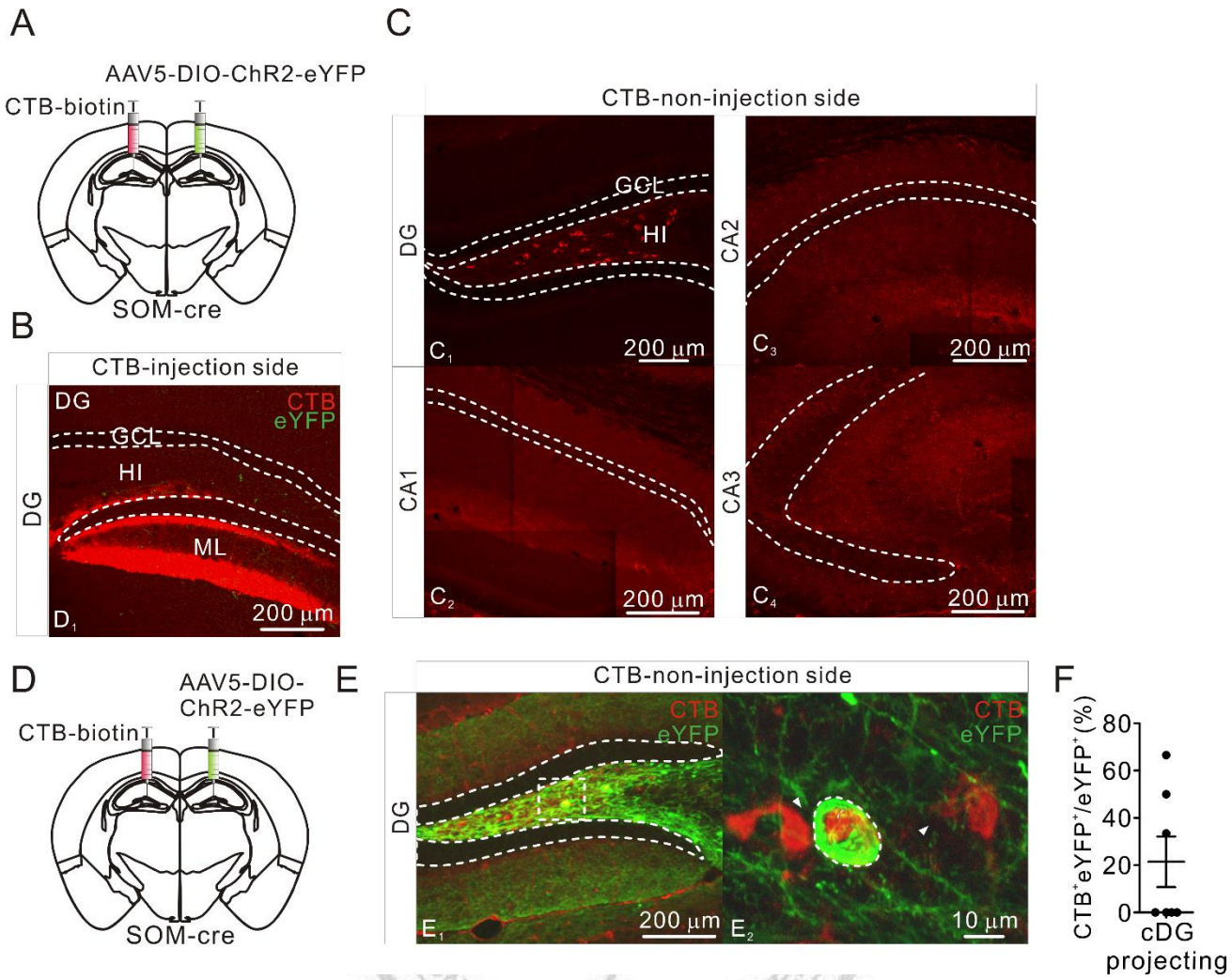

Figure 3. Somatic location of long-range projecting SOM$^+$ neurons

A, schema of the retrograde tracer (CTB-biotin) and AAV5 injection into the left and right dorsal DG, respectively. B, expression of CTB (red) in the ML of the injected site (also denoted as "CTB-injected site" side here). C, fluorescence image of retrograde tracer CTB-labelled cells in the CTB-non-injected hilus. C, CTB-labelled cells were detected in the DG (C_1), but not in the CA1 (C_2), CA2 (C_3), and CA3 (C_4) areas of CTB-non-injected site. D, schema of the retrograde tracer (CTB-biotin) and AAV5 injection into the left and right dorsal DG, respectively. E, CTB$^+$ and/or eYFP$^+$ cells in the AAV5 injected site. The enlargement of dashed box is shown in E_2. E_2, example of a both CTB$^+$ and eYFP$^+$

cell (see dashed circle). Note that there are two CTB^+ but $eYFP^-$ cells (see arrowhead). F, proportion of CTB^+-$eYFP^+$ cells of all $eYFP^+$ cells in the DG.

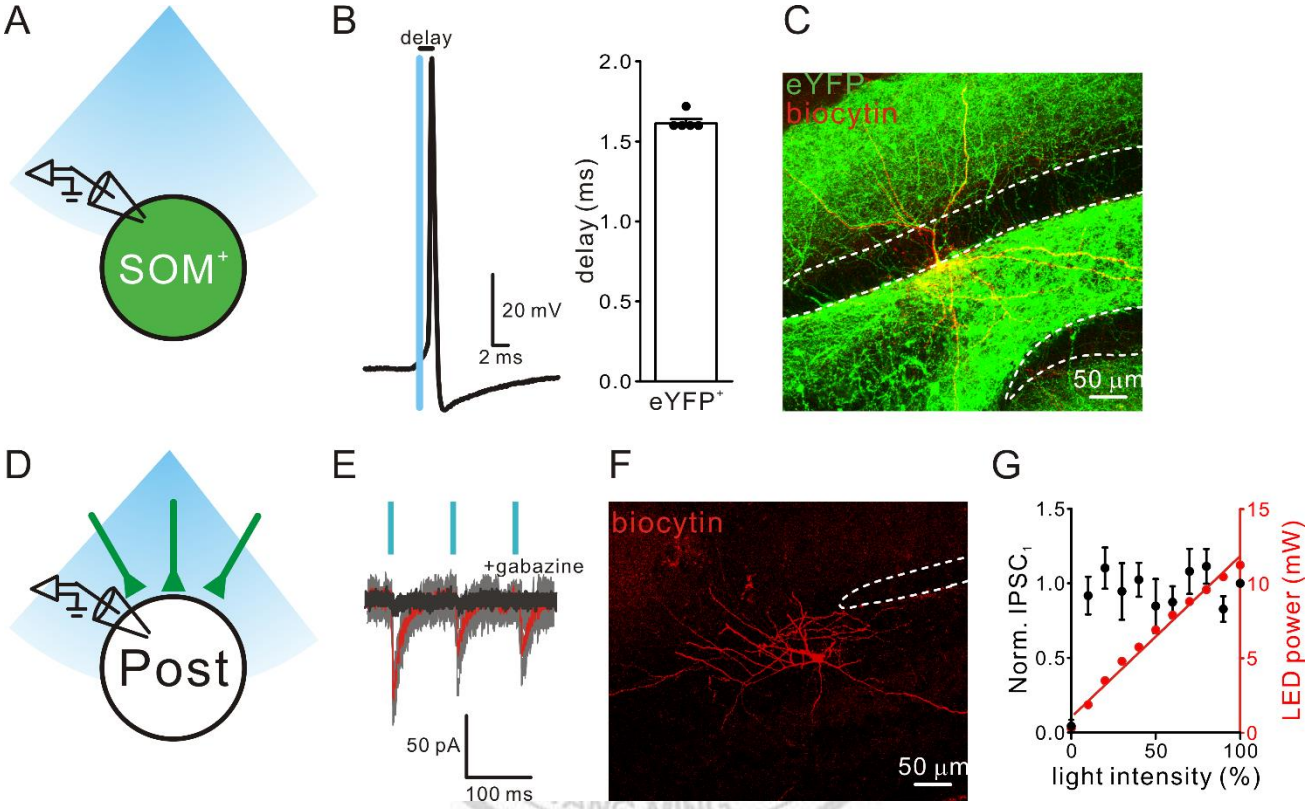

Figure 4. Optical activation of SOM$^+$ neurons and evoked post-synaptic responses

A, experimental schema showing optical activation of a recorded ChR2-expressing neuron by blue light pulses (470 nm). B, left: action potential was evoked in the eYFP$^+$ neuron (C) by an 1-ms blue (470 nm) light pulse (blue line). Right: the averaged delay from the light onset to the peak of action potential (as indicated in left panel). C, an example of biocytin-filled (red) eYFP$^+$ neuron in the border of the GCL and hilus. The axonal arborization was mainly distributed in the OML, suggesting a putative HIPP IN. D, schema of optical activation (470 nm blue light) of SOM$^+$ axons and recording of postsynaptic responses. E, a series of 3 light pulses at 10 Hz were delivered and light-evoked IPSCs

(red, average from 4 traces; gray, individual traces) were recorded in an IN (the same cell as in F) in voltage-clamp mode (at -70 mV); the IPSCs were blocked by gabazine (1 μM) (black traces). F, stacked two-photon image of a biocytin-filled IN (red) in the DG hilus. G, the plot showing normalized $IPSC_1$ amplitude (left ordinate) and absolute LED intensity (right ordinate) versus relative LED light intensity (abscissa).

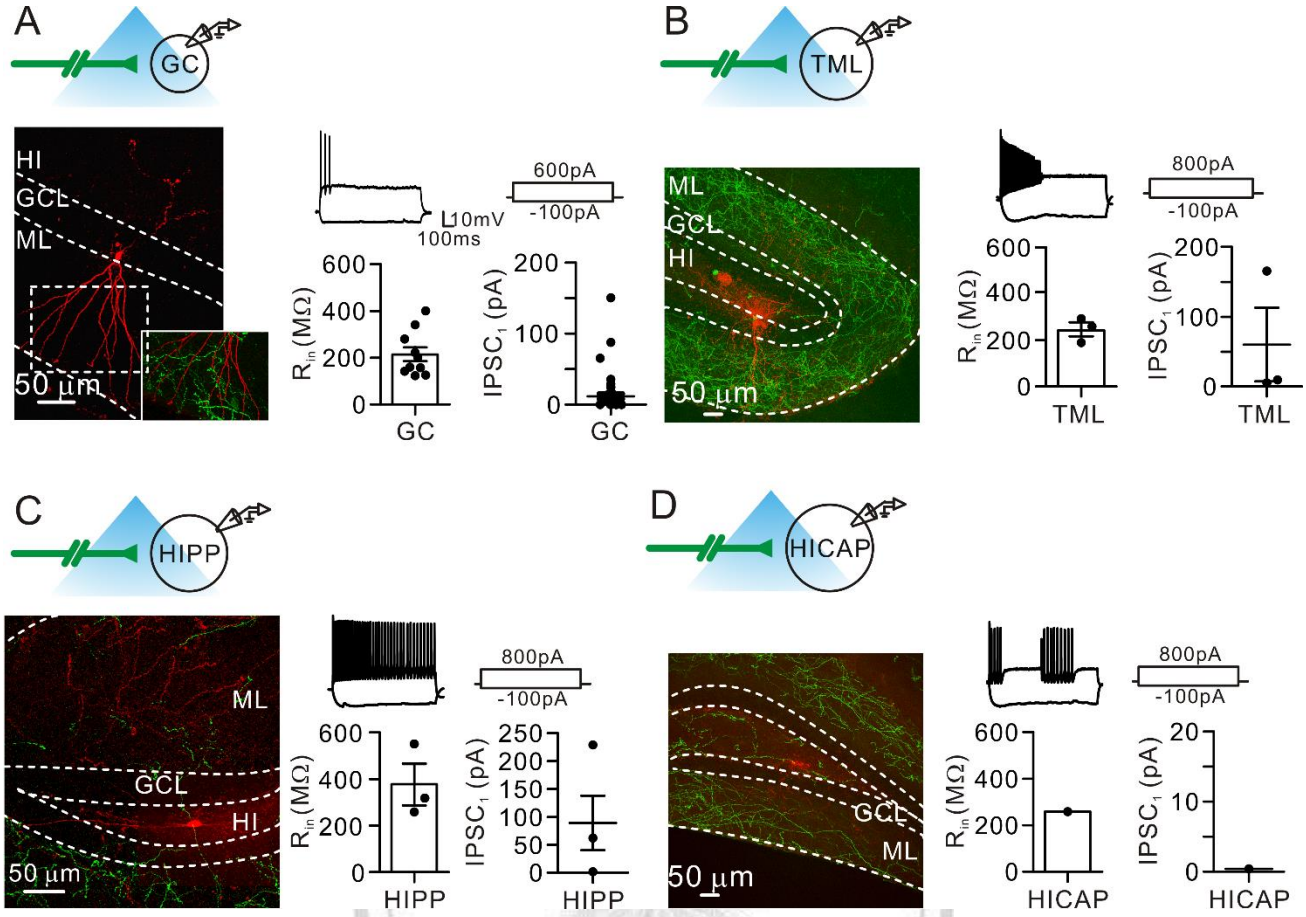

Figure 5. Morphologically identified GCs and subtypes of INs in the contralateral DG

A-D, upper: optogenetic stimulation of long-range SOM^+ axons with patch-clamp recordings from cGCs, cTMLs, cHIPPs, and cHICAPs respectively. Lower left: two-photon images of biocytin-filled (red) cGC (A), cTML (B), cHIPP (C), and cHICAP (D), the long-range axons were indicated with eYFP signals (green). Lower right: firing patterns and hyperpolarized membrane responses (induced by the protocol shown in the right) of cGCs (A), cTMLs (B), cHIPPs (C), and cHICAP (D) respectively. The R_{in} and $IPSC_1$ were plotted in each panel.

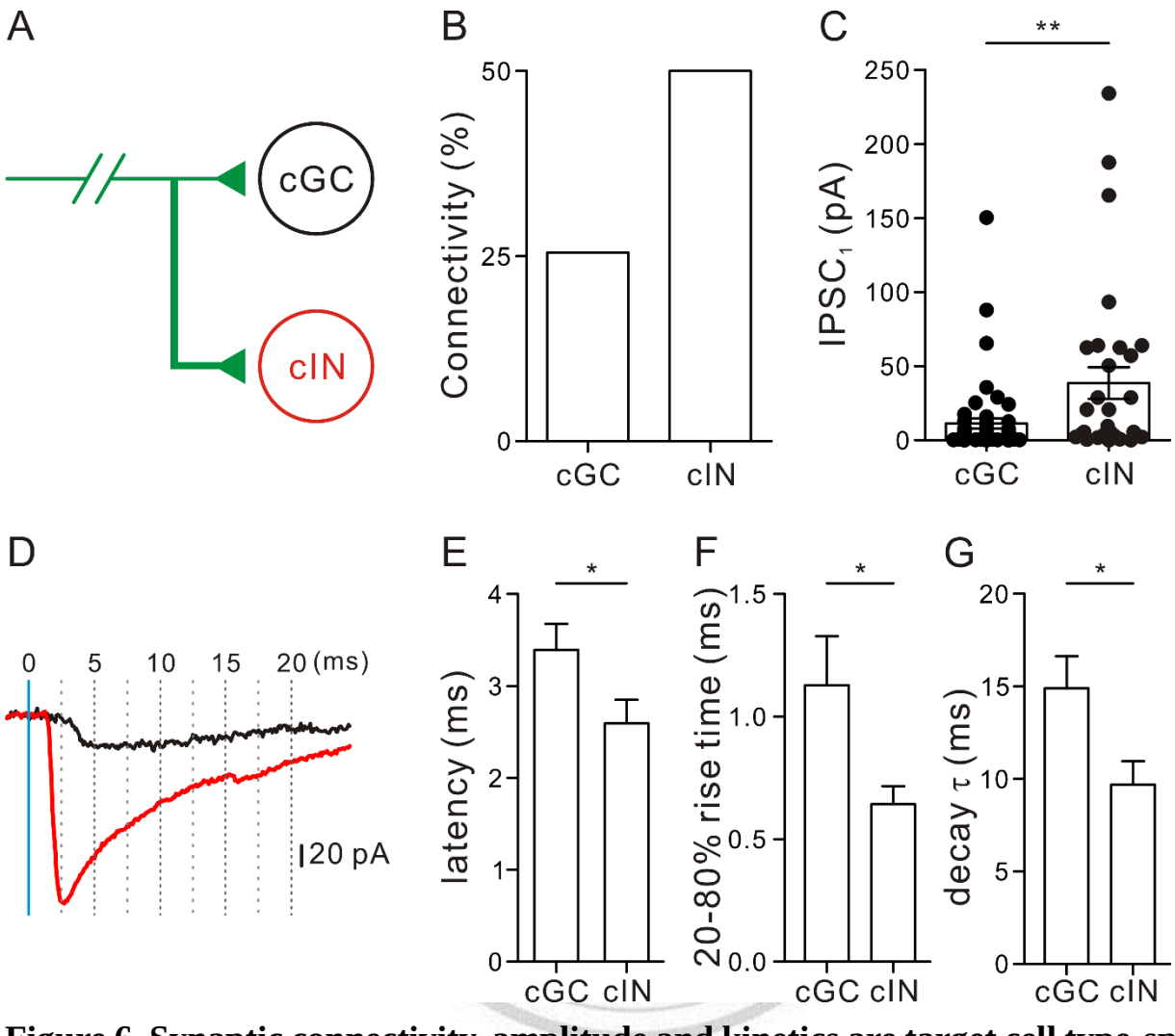

Figure 6. Synaptic connectivity, amplitude and kinetics are target cell type-specific

A. Schematic wiring of the SOM$^+$ neurons to cGCs and cINs. B, connectivity of long-range SOM$^+$ cells to cGCs (25.5%, 13 of 51 cells) and cINs (50%, 16 of 32 cells), C, Average $IPSC_1$ recorded in cINs is significantly larger than that recorded in cGCs. D, the first blue light pulse (blue line) and their corresponding average IPSCs recorded from cGC (black trace; average of 8 individual traces) and cIN (red trace; average of 26 individual traces). E-G, bar graphs showing that cIN output synapses displayed shorter synaptic latencies, faster rise and decay times than those in cGCs. *$p < 0.05$; **$p < 0.001$; MWW test.

Figure 7. Red Retro Beads-expressing hilar cell in the Beads-non-injected site

One of the Red Retro Beads-expressing neuron, the Retro Beads were mostly distributed in the somatic region, and its firing pattern.

References

Andrews-Zwilling Y, Gillespie AK, Kravitz AV, Nelson AB, Devidze N, Lo I, Yoon SY, Bien-Ly N, Ring K, Zwilling D, Potter GB, Rubenstein JLR, Kreitzer AC, Huang Y (2012) Hilar GABAergic interneuron activity controls spatial learning and memory retrieval. PloS One 7:1-12.

Bartos M, Vida I, Frotscher M, Meyer A, Monyer H, Geiger JR, Jonas P (2002) Fast synaptic inhibition promotes synchronized gamma oscillations in hippocampal interneuron networks. Proc Natl Acad Sci USA 99:13222-13227.

Buzsáki G, Draguhn A (2004) Neuronal oscillations in cortical networks. Science 304:1926-1929.

Chiu CQ, Lur G, Morse TM, Carnevale NT, Ellis-Davies GC, Higley MJ (2013) Compartmentalization of GABAergic inhibition by dendritic spines. Science 340:759-762.

Cobb SR, Buhl EH, Halasy K, Paulsen O, Somogyi P (1995) Synchronization of neuronal activity in hippocampus by individual GABAergic interneurons. Nature 378:75-78.

Freund TF, Buzsáki G (1996) Interneurons of the hippocampus. Hippocampus 6:347-470.

Freund TF, Katona I (2007) Perisomatic inhibition. Neuron 56:33-42.

Bartos M, Vida I, Jonas P (2007) Synaptic mechanisms of synchronized gamma oscillations in inhibitory interneuron networks. Nat Rev Neurosci 8:45-56.

Geiger JRP, Jonas P (2000) Dynamic control of presynaptic Ca^{2+} inflow by fast-inactivating K^{+} channels in hippocampal mossy fiber boutons. Neuron 28:927-939.

Glickfeld LL, Scanziani M (2006) Distinct timing in the activity of cannabinoid-sensitive and cannabinoid-insensitive basket cells. Nat Neurosci 9:807-815.

Hosp JA, Strüber M, Yanagawa Y, Obata K, Vida I, Jonas P, Bartos M (2014) Morpho-physiological criteria divide dentate gyrus interneurons into classes. Hippocampus 24:189-203.

Ishizuka N (2001) Laminar organization of the pyramidal cell layer of the subiculum in the rat. J Comp Neurol 435:89-110.

Klausberger T, Somogyi P (2008) Neuronal diversity and temporal dynamics: the unity of hippocampal circuit operations. Science 321:53-57.

Klaushaar U, Jonas P (2000) Efficacy and stability of quantal GABA release at a hippocampal interneuron-principal neuron synapse. J Neurosci 20:5594-5607.

Liu YC, Cheng JK, Lien CC (2014) Rapid dynamic changes of dendritic inhibition in the dentate gyrus by presynaptic activity patterns. J Neurosci 34:1344-1357.

Melzer S, Michael M, Caputi A, Eliava M, Fuchs EC, Whittington MA, Monyer H (2012) Long-range-projecting GABAergic neurons modulate inhibition in hippocampus and entorhinal cortex. Science 335:1506-1510.

Miles R, Tóth K, Gulyás AI, Hájos N, Freund TF (1996) Differences between somatic and dendritic inhibition in the hippocampus. Neuron 16:815-823.

Naber PA, Witter MP (1998) Subicular efferents are organized mostly as parallel projections: a double-labeling, retrograde-tracing study in the rat. J Comp Neurol 393:284-297.

Nakishiba T, Young JZ, McHugh TJ, Buhl DL, Tonegawa S (2008) Transgenic inhibition of synaptic transmission reveals role of CA3 output in hippocampal learning. 319:1260-1264.

Nörenberg A, Hu H, Vida I, Bartos M, Jonas P (2010) Distinct nonuniform cable properties optimize rapid and efficient activation of fast-spiking GABAergic interneurons. Proc Natl Acad Sci USA 107:894-899.

O'Keefe J, Nadel L (1978) The hippocampus as a cognitive map. Oxford Clarendon press.

Peng Z, Zhang N, Wei W, Huang CS, Cetina Y, Otis TS, Houser CR (2013) A Reorganized GABAergic circuit in a model of epilepsy: Evidence from optogenetic labeling and stimulation of somatostatin interneurons. J Neurosci 33:14392-14405.

Pouille F, Scanziani M (2001) Enforcement of temporal fidelity in pyramidal cells by somatic feed-

forward inhibition. Science 293:1159-1163.

Ribak CE, Seress L, Peterson GM, Seroogy KB, Fallon JH, Schmued LC (1986) A GABAergic inhibitory component within the hippocampal commissural pathway. J Neurosci 6:3492-3498.

Rollenhagen A, Sätzler K, Rodríguez EP, Jonas P, Frotscher M, Lübke JHR (2007) Structural determinnts of transmission at large hippocampal mossy fiber synapses. J Neurosci 39:10434-10444.

Savanthrapadian S, Meyer T, Elgueta C, Booker SA, Vida I, Bartos M (2014) Synaptic properties of SOM- and CCK- expressing cells in dentate gyrus interneuron networks. J Neurosci 34:8197-8209.

Schaffer K (1892) Beitrag zur histologie der Amnionshornformation. Arch Mikrosk Anat 39:611-632.

Scoville WB, Milner B (1957) Loss of recent memory after bilateral hippocampal lesions. J. Neurol. Neurosurg. Psychiat 20: 11-21.

Szirmai I, Buzsáki G, Kamondi A (2012) 120 years of hippocampal schaffer collaterals. Hippocampus 22:1508-1516.

Xu H, Jeong HY, Tremblay R, Rudy B (2013) Neocortical somatostatin-expressing GABAergic interneurons disinhibit the thalamorecipient layer 4. Neuron 77:155-167.

Zappone CA, Sloviter RS (2001) Commissurally projecting inhibitory interneurons of the rat hippocampal dentate gyrus: a colocalization study of neuronal markers and the retrograde tracer fluoro-gold. J Comp Neurol 441:324-344.